Checkpoint adaptation in repair-deficient cells drives aneuploidy and resistance to genotoxic agents

Katharina Bender[1,2*], Olga Vydzhak[1,2*], Julia Klermund[1], Anke Busch[1], Stefanie Grimm[1,2], and Brian Luke[1,2,4]

[1]Institute of Molecular Biology (IMB); Mainz, 55128; Germany

[2]Johannes Gutenberg University Mainz; Faculty of Biology, Institute of Developmental Biology and Neurobiology; Mainz, 55128; Germany

[*]These authors contributed equally

[4]Correspondence: b.luke@imb-mainz.de

Abstract

Human cancers frequently harbour mutations in DNA repair genes, rendering the use of DNA damaging agents as an effective therapeutic intervention. As therapy-resistant cells often arise, it is important to better understand the molecular pathways that drive resistance in order to facilitate the eventual targeting of such processes. We employ repair-defective diploid yeast as a model to demonstrate that, in response to genotoxic challenges, nearly all cells eventually undergo checkpoint adaptation, resulting in the generation of aneuploid cells with whole chromosome losses that have acquired resistance to the initial genotoxic challenge. We demonstrate that adaptation inhibition, either pharmacologically, or genetically, drastically reduces the occurrence of resistant cells. Additionally, the aneuploid phenotypes of the resistant cells can be specifically targeted to induce cytotoxicity. We provide evidence that TORC1 inhibition with rapamycin, in combination with DNA damaging agents, can prevent both checkpoint adaptation and the continued growth of aneuploid resistant cells.

Keywords

Checkpoint adaptation, rapamycin, aneuploidy, resistance, genome instability, DNA repair

Introduction

To preserve genome stability, eukaryotic cells have developed elaborate, and highly conserved, mechanisms to deal with DNA damage. In response to double-strand breaks (DSBs), a signalling cascade termed the DNA damage checkpoint (DDC) is activated to arrest the cell cycle before sister chromatid segregation occurs (reviewed in [1]). The DDC is essential to prevent the propagation of cells with damaged chromosomes, which leads to genome instability, as well as providing time for the repair of the damaged DNA. The main steps in DDC activation in *Saccharomyces cerevisiae* comprise nucleolytic processing by the MRX complex and other nucleases [2-4] to allow recognition of the damage site via Mec1/Ddc2 [5]. Subsequently, Mec1 activates the checkpoint effector kinases Rad53 and Chk1 utilizing the checkpoint mediator Rad9 [6-8]. To achieve a cell cycle arrest, Rad53 targets securin/Pds1 to prevent sister chromatid separation [9] and inhibits the pro-mitotic kinase Cdc5 [10-13], the yeast homologue of human Polo-like kinase 1 (PLK1) [14]. In addition, Rad53 triggers a transcriptional response to DNA damage [15-17].

Repair of DSBs is facilitated by two major pathways, namely homologous recombination (HR) and non-homologous end joining (NHEJ). The choice between these pathways is influenced by the cell cycle stage and hence the ability to resect the broken DNA ends, as well as the ploidy state [18]. Diploid yeast cells actively suppress NHEJ throughout the cell cycle on the transcriptional level, rendering them dependent on HR to repair DSBs [19-21]. To engage in HR, DSB ends are resected and rapidly bound by the ssDNA binding protein RPA [3,22]. Rad52, which is essential for HR-mediated repair in yeast, then promotes the replacement of RPA with the recombinase Rad51 [23,24]. Rad52-mediated loading of Rad51 is assisted by Rad55 and Rad57 [25]. The Rad51-ssDNA nucleoprotein filament then scans the genome for intact homologous template sequences to drive the error-free repair reaction[26,27,28]. Following successful DNA repair, the checkpoint is eventually extinguished and cells are able to continually divide, a process referred to as checkpoint recovery [29,30].

In certain scenarios, DNA damage can be considered irreparable as dictated by the nature of damage, i.e. where the damage occurs (e.g. telomeres), or the genetic context of the cell (e.g. loss of *RAD52* in diploid yeast). In response to persistent damage, DDC signalling can however still be terminated, in a process termed checkpoint adaptation [31,32]. Checkpoint adaptation is considered to be a last effort to maintain cell viability and avoid cell death by attempting to either tolerate the DNA damage load, or repair by alternative means [33]. In response to genotoxic stress and dysfunctional telomeres, checkpoint adaptation precedes genomic instability [34, 35] and

facilitates the use of mutagenic repair pathways including break-induced replication (BIR) [34]. Importantly, checkpoint adaptation has been documented in both uni- and multicellular systems including budding yeast, *Xenopus* egg extracts, plant and cancer cells [31,32,36-40]. One striking similarity in the process of checkpoint adaptation across all organisms is the critical contribution of PLK1 [41,42] and its homologues such as budding yeast Cdc5 [31]. An allele of *CDC5* (*cdc5-ad*), which harbours a single point mutation (L251W), is specifically defective in checkpoint adaptation [31]. The nutritional status of a cell can also impact the decision to undergo checkpoint adaptation [43]. More specifically, inhibition of the highly conserved TOR complex 1 (TORC1) by rapamycin treatment was shown to prevent checkpoint adaptation in response to chronic dysfunctional telomeres [43]. TORC1 not only promotes checkpoint adaptation in the presence of unrepaired DNA damage [43] but also enables chromosome mis-segregation by activating the Glc7/PP1 phosphatase, an opponent of the spindle assembly checkpoint (SAC) protein, Ipl1 [44].

It has long been recognized that yeast cells lacking Rad52 experience extensive chromosome loss after irradiation [45], however direct links to checkpoint adaptation have not been drawn. Extensive studies on yeast and mammalian cells with abnormal chromosome numbers (aneuploid cells) have identified a common aneuploidy-associated phenotype characterized by increased levels of proteotoxic stress resulting from imbalanced protein expression [46-50], delayed cell cycle progression [51-53], metabolic stress [47,48], non-genetic heterogeneity between clones [51] as well as increased and persistent DNA damage [54,55]. Many of these phenotypes that exist in aneuploids are susceptible to being targeted by pharmacological agents [48].

In this study, we have used repair-defective diploid yeast as a model to better understand the consequences of checkpoint adaptation following a challenge with clinically relevant genotoxic agents. We observe that the re-growth of repair-defective cells almost exclusively depends on checkpoint adaptation. All of the adapted cells that we characterized had undergone chromosome loss, rendering them aneuploid, and had acquired resistance to further DNA damaging agents. By combining genotoxins with inhibitors of checkpoint adaptation or with aneuploidy-selective agents, we were able to synergistically enhance the cytotoxicity of repair-defective cells, while repair-proficient cells remained unscathed. These results suggest that combination therapies targeting checkpoint adaptation and aneuploidy-associated phenotypes together with conventional DNA damaging chemotherapeutics, may be considered in human cancers with mutations in DNA repair genes.

Results

Checkpoint adaptation drives resistance to genotoxic challenge

To better characterise the cellular consequences of checkpoint adaptation, we established a model where adapted cells could be recovered in a reproducible manner for further analysis. To this end, a previous study has demonstrated that diploid repair-deficient *rad52* mutants readily undergo checkpoint adaptation following exposure to X-rays [34]. We performed similar experiments by treating repair-defective homozygous diploids, deleted for the *RAD52* gene, with camptothecin (CPT), which induces double-strand breaks (DSBs) by trapping Top1 cleavage complexes (Top1cc) on the DNA [56]. As expected, in the presence of CPT, *rad52* cells were unable to form colonies on agar plates after 2 days, unlike wild type cells or unchallenged *rad52* cells (Fig. 1a and data not shown). Following 5 days of incubation, small colonies began to form, which were clearly visible after 8 days (Fig. 1a). Despite their growth, the colonies contained a large fraction of metabolically inactive cells as indicated by the accumulation of the vital dye Phloxine B (pink colouring) [57]. Colony formation was not a result of decreased CPT activity over time, as CPT-containing plates incubated at 30°C for 7 days were as effective in killing *rad52* cells as freshly prepared plates (Supplementary Fig. 1a). Quantification of cell survival normalized to "no drug" control plates revealed that approximately 85 % of the plated *rad52* mutants were able to eventually form colonies following prolonged incubation on CPT solid agar plates (Fig. 1b). To demonstrate that checkpoint adaptation was responsible for the growth of repair-defective *rad52* cells on CPT, we introduced the adaptation-defective *cdc5-ad* allele [31]. Survival of adaptation-deficient *rad52 cdc5-ad* mutants was strongly reduced (to approximately 30 %, Fig. 1a, b), suggesting that checkpoint adaptation is required for the delayed colony formation. In cells that were repair competent, the presence of the *cdc5-ad* allele had no effect on viability following CPT challenge (Fig. 1a, b). Similar results were obtained when X-rays were used as a source of DNA damage (Fig. 1c, Supplementary Fig. 1b) as previously described [34]. In response to the radiomimetic drug bleomycin, adaptation-deficient *rad52 cdc5- ad* cells were also significantly sensitized to the drug treatment compared to *rad52 CDC5* mutants (Supplementary Fig. 1c). Therefore, Cdc5-mediated checkpoint adaptation promotes the delayed survival and growth of repair-defective cells following genotoxic stress.

To confirm that the *cdc5-ad* associated decreased viability was a result of checkpoint maintenance, we employed the checkpoint-defective *rad53-11* allele [8] to see if it would abolish the enhanced sensitivity phenotype. Indeed, preventing adaptation in *rad52 cdc5-ad* mutants

was only able to decrease viability following CPT or X-ray treatment in a checkpoint-competent *RAD53* background but not in *rad53-11* cells (Fig. 1d, e).

To investigate if adapted *rad52* mutants that were able to eventually survive genotoxic stress had acquired drug resistance, we exposed the adapted cells to a second genotoxic challenge. As shown in Fig. 1f, adapted repair-defective mutants derived from CPT-containing plates (*rad52* (CPT)) displayed a significant growth advantage as compared to *rad52* cells that had not been previously exposed to CPT (*rad52* (YPD)). The few *rad52 cdc5-ad* cells that had adapted also acquired drug resistance. Similar drug resistance was observed in adapted cells that had been exposed to X-rays, however, these cells remained sensitive to CPT (Supplementary Fig. 1d). Together, these results suggest that the development of genotoxin resistance in repair-defective cells is promoted by checkpoint adaptation.

Rapamycin can prevent checkpoint adaptation in repair defective cells

We have previously demonstrated that treating cells with the TORC1 inhibitor rapamycin, prevents checkpoint adaptation in response to DNA damage arising from chronic dysfunctional telomeres [43]. To determine whether rapamycin was also able to prevent checkpoint adaptation in diploid *rad52* cells after genotoxic treatment, we analysed cell division in a microcolony assay. G1 or S phase cells were micromanipulated onto agar plates containing the indicated drugs and checkpoint adaptation was scored as the appearance of microcolonies consisting of more than 2 or 4 cell bodies (Fig. 2a) [31,58]. The presence of rapamycin significantly reduced the frequency of checkpoint adaptation in response to both X-ray (Fig. 2b) and CPT treatment (Fig. 2c) in repair-defective *rad52* mutants. Even in the absence of exogenous damage (first bar Fig. 2b, c) rapamycin slightly reduced the formation of microcolonies, presumably due to irreparable endogenous damage occurring in *rad52* mutants.

To test the effects on cell survival, we concomitantly exposed *rad52* cells to rapamycin and CPT, which resulted in approximately 25 % cell survival of *rad52* mutants compared to approximately 94 % survival after CPT treatment alone (Fig. 2d). In contrast to the *cdc5-ad* allele (Fig. 1d, e), the decrease in cell survival due to rapamycin was not reversed when the checkpoint was compromised by introducing the *rad53-11* allele (Fig. 2d) [8]. Moreover, the presence of rapamycin led to an additive effect in decreasing cell survival of adaptation-deficient *rad52 cdc5-ad* mutants (Fig. 2e). Similar results were obtained when using X-rays as a source of DNA damage instead of CPT (Supplementary Fig. 2a, b).

In summary, rapamycin, like the *cdc5-ad* allele, is able to prevent checkpoint adaptation in repair-defective cells exposed to genotoxic agents. Furthermore, the strong loss of viability

when combining either rapamycin (Fig. 2d, e, Supplementary Fig. 2a, b) or *cdc5-ad* (Fig. 1b, c) with genotoxic agents is specific to repair-defective cells, as repair-proficient cells remain fully viable. Unlike the *cdc5-ad* allele, rapamycin is also able to impart toxicity in a checkpoint-independent manner (Fig. 2d, Supplementary Fig. 2a), which can account for the additive cytotoxicity when *rad52 cdc5-ad* cells are exposed to rapamycin in the presence of genotoxins (Fig. 2e, Supplementary Fig. 2b).

Adapted repair-defective cells become aneuploid

In the absence of *RAD52*, chromosome loss is frequently observed and this is exacerbated upon X-ray treatment [45]. Consistently, DNA content analysis of adapted *rad52* mutants after genotoxic treatment revealed a high degree of chromosome loss resulting in aneuploid cells ranging from near diploid to near haploid DNA contents (Fig. 3a). By employing a whole-genome sequencing approach on the strains depicted in Fig. 3a, we were able to conclude that the aneuploidy was a result of whole chromosome loss events (Fig. 3b). Accordingly, pulsed-field gel electrophoresis indicated that in our conditions, gross chromosomal rearrangements were not occurring in the adapted cells (Supplementary Fig. 3a). Following CPT treatment of *rad52* cells we observed the loss of one copy of nearly all chromosomes, with the exception of chromosome III (Fig. 3b). This DNA content was stably maintained over several rounds of passaging (not shown). In contrast, X-ray irradiation produced *rad52* mutants with a variety of karyotypic changes ranging from extensive chromosome loss to individual loss events (Fig. 3a, b, lower 3 karyotypes). Although representative DNA content analyses for only 5 adapted strains are depicted in Figure 3a, this was highly reproducible in the over 50 adapted clones that were tested for DNA content (data not shown). Preventing adaptation in a *cdc5-ad* genetic background largely impaired the regrowth of repair-defective cells following genotoxic stress (Fig. 1b, c), however, it was not completely abolished, and the rare *rad52 cdc5-ad* mutants that were able to form colonies also underwent extensive chromosome loss (Supplementary Fig. 3b). To rule out that the reduction in chromosome numbers may have occurred through the induction of meiosis, we deleted the *SPO11* gene in *rad52* mutants [59], and exposed them to CPT. In the meiosis-defective cells, we observed that the number of adapted cells was not altered (Supplementary Fig. 3c), and moreover, the aneuploid karyotype remained prevalent (Supplementary Fig. 3d).

The phenotypes associated with aneuploidy in yeast have largely been described based on the experimental creation of disomic strains [47,49,60,61]. We tested whether checkpoint adapted aneuploids display similar phenotypes. Due to imbalances in protein complexes disomic strains

are defective in maintaining proteostasis, which can be visualized by the inability to resolve Hsp104-GFP positive protein aggregates following heat challenge [49]. Indeed, checkpoint adapted aneuploids (derived from X-ray irradiation) were impaired in resolving Hsp104-GFP foci following 3 hours at 37 °C, when compared to naiive *rad52* mutants and wild type cells (Fig. 3c, d). Consistently, many of these X-ray adapted aneuploids were severely impaired for growth at 37 °C, which correlated with their ability to resolve Hsp104-GFP foci (Fig. 3e). The cells that adapted from CPT treatment, which were almost exclusively disomic for chromosome III, but otherwise haploid, did not show defects in Hsp104-GFP foci resolution, nor were they impaired for growth at 37 °C (Supplementary Fig. 3e, f, g).

In summary, following checkpoint adaptation, the resistant cells that arise undergo extensive chromosome loss and a sub-set of them display aneuploidy-associated phenotypes similar to laboratory-derived disomes.

Checkpoint adapted aneuploids can be targeted pharmacologically

The fact that aneuploid cells display proteotoxic stress opens an opportunity to target proteostasis regulators in order to induce cytotoxicity [46-49]. We treated adapted aneuploids with low doses of the proteasome inhibitor, MG132, and observed a striking effect on population doubling time as compared to naiive wild type or *rad52* cells (Fig. 4a). Consistent with the fact that adaptation to CPT did not result in defective Hsp104-GFP foci resolution following heat stress (Supplementary Fig. 3e, f), they did not show enhanced sensitivity to MG132 (Supplementary Fig. 4a). Apart from sensitivity to proteostatic perturbations, aneuploid cells have also been reported to have altered energy demands, hence rendering them sensitive to TORC1 inhibitors, such as rapamycin [47,48]. Indeed, adaptation following X-ray treatment rendered cells hyper-sensitive to low doses of rapamycin (Fig. 4b). Adaptation to CPT did not result in rapamycin resistance (Supplementary Fig. 4b). It has been previously reported that aneuploid cells display characteristic but extremely heterogeneous response patterns after stress [51], which can be clearly observed in the reactions to MG132 (Fig. 4a) and rapamycin (Fig. 4b). We directly compared the deviations between growth rates in unchallenged conditions and could confirm that there is significant difference between adapted cells and naiive *rad52* mutants (Fig. 4c).

To further understand the nature of the rapamycin sensitivity, we monitored TORC1 activity in checkpoint adapted cells by following the levels of phosphorylated Sch9 (p-Sch9), a direct target of TORC1 [62]. Whereas TORC1 activity was already reduced in naiive *rad52* cells compared to wild type, the checkpoint adapted aneuploids had even further reduced levels of

p-Sch9 (Fig. 4d). Moreover, using the GFP-Atg8 reporter [48], we observed increased levels of autophagy in X-ray adapted cells (Fig. 4e) but not in CPT adapted cells (Supplementary Fig. 4c), consistent with the respective rapamycin sensitivity.

In summary, these data demonstrate that although adapted cells acquire genotoxin resistance, their aneuploid status renders them sensitive to agents that target proteostasis and energy regulation pathways.

CPT adapted cells rely on MRX-mediated DNA damage repair

We next set out to address why checkpoint adapted cells become resistant to further genotoxic challenges. In order to test if adapted *rad52* mutants were still checkpoint-proficient following an adaptation event, we challenged mutants derived from either CPT-containing plates or irradiated with 45 Gy for a second time with CPT (Fig. 5a) and 45 Gy (Supplementary Fig. 5a), respectively. To monitor DNA damage checkpoint activation, we followed the phosphorylation-dependent mobility shift of Rad53 [63] as well as the induction of ribonucleotide reductase 3 (Rnr3) expression [64]. We observed that all adapted *rad52* mutants had a basal activation of the DNA damage checkpoint, however they were still proficient in checkpoint activation following exposure to the respective DNA damaging agent, ruling out the notion that a faulty checkpoint may allow for the resistance phenotype.

We therefore tested whether an alternative repair mechanism would allow the survival of post-adaptation *rad52* mutants [65,66]. In addition to homologous recombination, non-homologous end joining (NHEJ) constitutes the second major DSB repair pathway. However, in diploid yeast strains, as used in our experiments, NHEJ is actively suppressed by the transcriptional repression of critical NHEJ factors [19-21]. Nevertheless, since the adapted cells lose chromosomes and resemble a more "haploid-like" karyotype, we sought to address if the survival of *rad52* mutants after genotoxic stress was facilitated by the aberrant use of NHEJ. To test this, we exposed *rad52* mutants lacking DNA ligase IV (Dnl4), a crucial NHEJ factor, to genotoxic stress. The absence of *DNL4* did not compromise cell survival of *rad52* mutants in the presence of CPT (Fig. 5b) or after X-ray irradiation (Supplementary Fig. 5b). We further investigated the involvement of other repair pathways and found that the deletion of either *RAD59, RAD51, RAD55, RAD1* or *POL4* did not hinder the formation of adapted colonies following either CPT or X-ray exposure in a *rad52* background (Supplementary Fig. 5c-g). Strikingly, the deletion of *MRE11,* prevented the growth of adapted cells in the presence of CPT (Fig. 5c, d), but not following X-ray exposure (Supplementary Fig. 5h). Another MRX (Mre11-Rad50-Xrs2)

component, Rad50, also contributed to the re-growth of CPT adapted cells (Supplementary Fig. 5i, j).

Since Mre11 does not contribute to adaptation *per se* [4], we considered that it may become essential for repair post-adaptation. To address this, we created an auxin-inducible degron (AID) version of Mre11 (Fig. 5e). We allowed *rad52* cells to adapt and form colonies in the presence of Mre11 and then assessed their sensitivity to CPT following auxin (IAA)-induced removal of Mre11. Indeed, we observed that adapted *rad52* cells acquire resistance to CPT in the presence of Mre11, but become sensitive following the subsequent removal of Mre11 (addition of IAA) (Fig. 5f). The sensitivity exceeds that of losing Mre11 in the presence of Rad52.

Together, these data suggest that the MRX complex contributes to the resistance phenotype of adapted *rad52* cells in response to chronic CPT exposure.

Discussion

Due to the fact that many human cancers harbour mutations in DNA repair genes, the use of genotoxic agents is frequently effective in the initial reduction of tumor size. Unfortunately, these treatments become ineffective as chemotherapy resistance develops. Therefore, it is essential to characterize the molecular events that occur when repair-defective cells are treated with genotoxins so that the pathways which lead to resistance can also be targeted in a combinatorial manner. We have employed repair-defective diploid yeast (*rad52/rad52)*, as a model to gain insights into these processes. Here, we demonstrate that in response to ionising radiation, as previously shown [34], and CPT treatment, checkpoint adaptation contributes to the eventual re-growth of cells. Importantly, the adapted cells that re-grow are resistant to further genotoxic challenges and undergo extensive whole chromosome losses (Figure 3), translocations and break-induced replication [34]. By preventing checkpoint adaptation through expression of *cdc5-ad,* or rapamycin treatment, the number of resistant colonies that form is drastically reduced. Moreover, rapamycin can also cause cytotoxicity in a post-adaptive manner, due to the aneuploid nature of the cells [47,48]. Taken together, we describe the sequence of events that occur when repair-defective cells acquire drug resistance, and demonstrate options for targeting them either genetically or pharmacologically.

Checkpoint adaptation allows the continued proliferation of cells, despite the presence of chromosomal damage [31,32]. Ideally, repair-competent cells should repair DNA damage before adaptation occurs (recovery), in order to prevent the risks associated with cell proliferation in the presence of lesions (Figure 6). In repair-proficient cells the inhibition of adaptation does not

have a negative effect on the sensitivity of the cells to DNA damage (Figure 1), in fact in the case of chronic telomere uncapping (*cdc13-1* cells), preventing adaptation is even advantageous for cell survival as long as the cells are given the opportunity to repair the damage [43]. When repair pathways are defective, the only option for cell survival following genotoxic stress is via checkpoint adaptation, therefore the inhibition of checkpoint adaptation in this scenario provides a synthetic lethal-like effect (Figure 6). The extrapolation of these findings to the scenario in human cancer suggests that the combination of adaptation inhibition with genotoxic drugs may give the desired effect of only causing cytotoxicity in the repair-defective tumor cells and not in the repair-proficient healthy tissue. In support of this notion, it has been demonstrated that BRCA1$^{-/-}$ breast cancer cells are hypersensitized to PARP inhibitors (PARPi) in the presence of rapamycin [67,68], although the role of checkpoint adaptation was not assessed in these studies. Furthermore, inhibition of PLK1 also leads to PARPi hypersensitization in BRCA1$^{-/-}$ cells [69].

Aneuploid cells experience proteotoxic stress due to imbalances in multi-subunit protein complexes, rendering them particularly sensitive to perturbations in protein quality control pathways [46-50]. Consistently we found that aneuploids resulting from adaptation were hypersensitive to the proteasome inhibitor, MG132. Adaptation-derived aneuploid cells were also sensitive to rapamycin (Figure 4), supposedly due to their altered energy demands owing to proteotoxic stress [47,53,70]. Therefore, rapamycin is particularly interesting as it can prevent checkpoint adaptation [43], but can also target aneuploids following adaptation (Figure 6). This explains the observations that in repair-defective cells exposed to genotoxins, rapamycin is additive with the adaptation-defective *cdc5-ad* allele (Fig. 2e) and is still prevents regrowth of checkpoint-defective cells (Fig. 2d). In contrast, the enhanced cytotoxicity of the *cdc5-ad* allele in *rad52* cells depends on the presence of the checkpoint, indicating that its action is solely through the DDC (Fig. 1d, e). Previous studies suggest that rapamycin inhibits Cdc5 function, which is likely how it prevents checkpoint adaptation [43,71]. How rapamycin specifically targets aneuploids remains enigmatic, although we have observed that TORC1 signalling is reduced in adapted cells as compared to naiive *rad52* and wild type cells (Fig. 4d, e).

Interestingly, CPT caused more extensive chromosome loss that X-ray treatment (Fig. 3b) whereby the CPT adapted cells were nearly exclusively disomic, having only one extra chromosome. X-ray adapted cells were very heterogeneous and were more “extreme” in the extent of their chromosome imbalances. This was also reflected in the extent of the sensitivity of the cells to proteotoxic stress and rapamycin (compare Fig. 3 and 4 with Supplementary Fig. 3 and 4). Consistently, in controlled experimental conditions, it has previously been observed

that a greater number of unbalanced chromosomes results in stronger aneuploidy-associated phenotypes [47,72]. It is interesting that chromosome III was consistently retained as the disomic chromosome in the CPT treated cells. Since the mating loci are on chromosome III, we speculate that this may have been a selection to prevent the mating of aneuploid cells, which would lead to further genome instability and likely cell death.

Importantly, aneuploidy *per se* does not render cells resistant to DNA damage [61] and hence we screened for candidate genes that may be responsible for the resistance emerging following adaptation. Indeed, we observed that the adapted cells rely on the MRX complex for their acquired resistance to CPT, but not to X-rays. Surprisingly, the resistance phenotype does not rely on compensation from other components of the HR machinery, including *RAD51, RAD55* and *RAD59* [65]. Therefore, inhibition of Mre11 in combination with CPT provides yet another opportunity to target repair defective cells and prevent the occurrence of aneuploid resistant cells. It has recently been demonstrated that cells undergoing replicative senescence due to telomere shortening also frequently adapt, which leads to subsequent genome instability[35]. It is tempting to speculate that by preventing adaptation, it may also lead to the elimination of senescent cell. In agreement, we have previously demonstrated that the longevity extension properties of rapamycin are partially dependent on the DNA damage checkpoint [43].

Taken together, we have used a yeast model to demonstrate the path taken by repair-defective cells in order to achieve drug resistance and by characterizing these cells, have elucidated ways to prevent their occurrence.

Methods

Spotting assay

Overnight cultures grown in YPD at 30 °C were spotted in tenfold serial dilutions starting with OD_{600nm} 0.5 in the first dilution onto the indicated agar plates. Images were taken after 3 to 4 days (unless indicated otherwise) using the ChemiDoc™ Touch Imaging System (Bio-Rad). Agar plates contained the vital dye Phloxine B at a final concentration of 8 µg/mL.

Western Blotting

Protein extraction was performed as described [43]. Briefly, cell pellets corresponding to 2 OD_{600nm} units were harvested by centrifugation and resuspended in 150 µL solution 1 (1.85 M NaOH, 1.09 M 2-mercaptoethanol) followed by incubation on ice for 10 min. After the addition of 150 µL of solution 2 (50 % TCA), the suspension was mixed briefly by vortexing and incubated on ice for 10 min. After clearing the samples by centrifugation at 13,000 rpm for 2 min at 4 °C, the pellet was washed in 1 mL acetone, centrifuged at 13,000 rpm for 2 min at 4 °C and resuspended in 100 µL urea buffer (120 mM Tris-HCl pH 6.8, 5 % glycerol, 8 M urea, 143 mM 2-mercaptoethanol, 8 % SDS, bromophenol blue). Resuspension was completed by incubation at 75 °C (or 50 °C when analysing Rad53 phosphorylation) for 5 min. If necessary, 1 M Tris-HCl at pH 7.5 was added to adjust the pH. Prior to loading, samples were centrifuged at 13,000 rpm for 1 min to precipitate insoluble material.

Proteins were separated on Mini-PROTEAN® TGX Stain-Free™ precast gels (Bio-Rad) using 7.5 % polyacrylamide gels for Rad53 detection or a gradient of 4-15 % polyacrylamide for all other proteins in Mini-PROTEAN® electrophoresis chambers (Bio-Rad). Proteins were transferred to 0.45 µm pore size nitrocellulose membranes (GE Healthcare) either by wet blot in transfer buffer (25 mM Tris, 192 mM glycine, 20 % ethanol) using Mini Trans-Blot® Cell chambers (Bio-Rad) or by semi-dry blot using the Trans-Blot® Turbo™ Transfer System (Bio-Rad) with the pre-set 10 min blotting program for high molecular weight proteins. Blocking was performed for at least 1 h at room temperature in 5 % skim milk/PBST (1.37 M NaCl, 0.03 M KCl, 0.08 M Na_2HPO_4 x 2 H_2O, 0.02 M KH_2PO_4, pH 7.4 supplemented with 0.1 % Tween-20) followed by incubation with the primary antibodies diluted in the same buffer over night at 4 °C. Membranes were incubated with secondary antibodies for 1 h (HRP-coupled antibodies) or 2 h (fluorescently-labelled antibodies) at room temperature. Proteins were visualized by chemiluminescence using ECL Western Blotting substrate (Pierce) on a

ChemiDoc™ Touch imaging system (Bio-Rad). Alternatively, proteins were detected on an Odyssey CLx Imaging system (Licor). All antibodies used are listed in Supplementary table 4.

DNA content analysis using flow cytometry

Cell pellets equivalent to 0.18 OD_{600nm} units were harvested by centrifugation, washed once in 1 mL water to remove medium and resuspended in 300 µL water. After fixation in 70 % ethanol, cells were centrifuged and washed in 1 mL water. After centrifugation, pellets were resuspended in 500 µL 50 mM Tris-HCl pH 7.5 containing 10 mg/mL RNase A and incubated at 37 °C for 3 h or overnight. After centrifugation, pellets were resuspended in 500 µL 50 mM Tris-HCl pH 7.5 containing 1 mg/mL Proteinase K and incubated at 50 °C for 45 min. Finally, cells were resuspended in 500 µL 50 mM Tris-HCl pH 7.5. Sonification was performed for 10 sec at level 1 using "constant" mode with a 3 mm sonification tip (Branson) or in a Bioruptor Pico (Diagenode) for 2 cycles 30 sec each. Subsequently, 500 µL 50 mM Tris-HCl pH 7.5 containing 2 µM Sytox Green were added (final concentration 1 µM), cells were transferred to FACS tubes (Falcon) and analysed on a FACSVerse flow cytometer (BD) using FACS Suite software (BD).

Creation of homozygous diploids

Isogenic haploids of mating type a or α, respectively, were transformed using a standard protocol with different plasmids conferring either antibiotic resistance or bearing auxotrophic markers (plasmids are listed in Supplementary Table 3). After mating under standard conditions, homozygous diploid selection was performed using the plasmid-borne markers.
For plasmid-free diploid selection, isogenic haploids were mated in liquid YPD medium at 30 °C for 5 h and diploids were picked based on morphology using a MSM 400 dissection microscope (Singer Instruments) followed by confirmation based on DNA content.

Genotoxic treatment procedures

For X-ray treatment, cells were irradiated with the indicated doses after plating on YPD agar plates using a 0.5 mm aluminium filter to remove low-energy X-rays. The dose rate was kept constant and was set to approximately 0.9 Gy/min at 130 kV and 5 mA. For further analysis, X-ray resistant colonies were picked directly from the irradiated plates.
For camptothecin treatment, cells were plated onto YPD agar plates containing the indicated drug concentration. After the formation of resistant colonies, they were patched onto YPD agar plates and afterwards used for further analysis.

Plating assay and statistical analysis of cell survival

Cells were taken from 5 mL overnight cultures in YPD at 30 °C and cell numbers per mL were assessed by counting in a Neubauer counting chamber. 300 cells were plated in 2 technical replicates and incubated at 30 °C for the indicated times. Plate images were taken with an Epson Perfection V700 scanner. Colonies were counted manually taking all colonies visible by eye into account and the average of the two technical replicates was used for further quantification. Colony numbers on plates with genotoxic treatment were normalized to number of colonies formed on control YPD plates and expressed as % survival. If not indicated otherwise, every quantification represents three biological replicates. Statistical analysis was performed using one-way ANOVA with Tukey's post-hoc test after confirming normal data distribution (Shapiro-Wilk test) and testing the heterogeneity of variances (Brown-Forsythe test) as built-in analyses in the Prism 7.02 software package (GraphPad). In the case of plating assays where genotype and treatment represented two different factors, normal data distribution and variance heterogeneity were tested as before. Subsequently, a two-way ANOVA was used to confirm statistically significant interaction between the two factors followed by Tukey's post-hoc test to report statistically significant differences between data sub-groups.

Microcolony assay

Cells were grown to saturation overnight in YPD medium at 30 °C. For X-rays as a damaging agent, cells were diluted 1:10 in fresh YPD and transferred to a petri dish followed by irradiation with 45 Gy. Afterwards, unbudded or small budded cells were manipulated onto YPD agar plates containing either 10 nM rapamycin (in DMSO) or DMSO. Based on a similar experiment performed in [31], microcolony formation was assessed by quantifying cell bodies, i.e. a cell arrest in G_2/M evident as a dumbbell shape was counted as 2 cell bodies. Microcolonies that contained only one cell body at the 4 h time point were excluded from further analysis. After 24 h, cell bodies present in every microcolony were counted. Cells were counted as adapted if the microcolony contained more than 2 cell bodies. Normal data distribution was tested using the Shapiro-Wilk test. Since data were not normally distributed, a Kruskal-Wallis test followed by Dunn's post-hoc test was employed. In the case of CPT as a damaging agent, cells were counted as adapted if the microcolony contained 3, 5 or more than 5 cell bodies. Four cell bodies were still considered arrested since a fraction of cells did not arrest with only 2 but 4 cell bodies at 4 h. This is due to a CPT-induced arrest in the next cell cycle if cells had already transitioned through S phase at the start of the experiment. Otherwise, quantification was performed in analogy to microcolony formation after X-ray.

Genomic DNA extraction

Exponentially growing cultures (20 mL of OD_{600nm} 0.7) were harvested by centrifugation, resuspended in 1 mL gDNA buffer 1 (0.9 M sorbitol, 0.1 M EDTA pH 7.5), transferred to a reaction tube and centrifuged at 13,000 rpm for 1 min. After resuspension in 400 µL of gDNA buffer 1 supplemented with 14 mM β-Mercaptoethanol, cell walls were digested by adding 20 µL of lyticase (2.5 mg/mL) for 45 min at 37 °C. Successful creation of spheroblasts was monitored with a light microscope. Subsequently, spheroblasted cells were centrifuged at 13,000 rpm for 1 min and resuspended in 400 µL 1x TE buffer. After addition of 90 µL gDNA buffer 2 (0.27 M EDTA pH 8.5, 0.44 M Tris, 2.2 % SDS), samples were vortexed briefly and incubated at 65 °C for 30 min. Subsequently, 80 µL of 5 M potassium acetate were added and samples were incubated at 4 °C for at least 1 h. Cell residues were eliminated by centrifugation at 14,000 rpm for 15 min at 4 °C and DNA contained in the supernatant was precipitated by addition of 750 µL cold 100 % ethanol. To facilitate precipitation, samples were incubated at - 20 °C for 30 min and subsequently centrifuged at 14,000 rpm for 5 min at 4 °C. After discarding the supernatant, DNA contained in the pellet was washed with 1 mL cold 70 % ethanol followed by air-drying the pellet at room temperature. DNA was resuspended gently in 500 µL 1x TE and incubated at 37 °C for 60 min in the presence of 2.5 µL RNase A (10 mg/mL). Subsequently, 500 µL isopropanol were added, the sample was mixed and centrifuged at 14,000 rpm for 15 min at 4 °C. After washing the pellet with 1 mL 70 % ethanol, DNA was air-dried at room temperature and resuspended gently in 50 µL 1x TE. Insoluble material was precipitated and removed following centrifugation at 14,000 rpm for 10 min at 4 °C.

DNA library preparation and sequencing

1 µg of genomic DNA was brought to a final volume of 50 µL and sheared using a Covaris S2 ultrasonicator system in a microTUBE AFA Fiber 6x16mm, applying the following shearing parameters: duty factor 10 %, intensity 5, 200 cycles per curst, 45 sec, 7 °C water bath temperature. After DNA shearing, a double-size selection was performed using Ampure XP beads with ratios of 0.6:1 (beads:DNA) to exclude larger fragments and 1:1 (beads:DNA) to remove smaller fragments. This procedure enriched the DNA for the 100-500 bp fragments. Purified DNA was quantified using the Qubit dsDNA HS Assay Kit in a Qubit 2.0 fluorometer (Life Technologies) and the DNA size distribution was profiled in a High Sensitivity DNA chip on a 2100 Bioanalyzer (Agilent Technologies).

DNA sequencing library preparation was performed using NuGEN´s Ovation Ultralow System V2 (2014-2017), following the manufacturer's recommendations. Libraries were prepared with

a starting amount of 80 ng of sheared DNA (100-500 bp in size) and were amplified in 8 PCR cycles. Libraries were profiled on a DNA 1000 chip on a 2100 Bioanalyzer (Agilent Technologies) and quantified using the Qubit dsDNA HS Assay Kit in a Qubit 2.0 fluorometer (Life Technologies).

DNA sequencing (DNA-seq) libraries were sequenced on Illumina NextSeq 500 (75-nt paired-end, with an effective read length of 79 nt), yielding 10-13 million read pairs per sample.

DNA sequencing analysis

Sequencing qualities were checked using FastQC (version 0.11.5) (https://www.bioinformatics.babraham.ac.uk/projects/fastqc/). All reads were mapped to the yeast genome (Ensembl genome assembly version R64) with the Burrows-Wheeler Aligner BWA (version 0.7.15) [73]. Reads not mapped in a proper pair as well as secondary alignments were removed using Samtools (version 1.3.1) [74]. Furthermore, duplicate reads were removed using MarkDuplicates of the Picard tool package (version 2.6.0) (http://broadinstitute.github.io/picard/). Due to very high and unequal coverage, the mitochondrial chromosome was removed from all subsequent analyses. Reads were counted and summarized in 1000 bp bins using readCounter of the HMMcopy package (version 0.1.1) ([75] and (https://github.com/shahcompbio/hmmcopy_utils)). Resulting wig files were transformed to bedgraph files using wigToBedGraph of the kentUtils package (version v302) without collapsing adjacent windows (https://github.com/ENCODE-DCC/kentUtils) and normalized to reads per million (PRM). Using a custom made R script, RPM of each bin were then normalized to the sample-wide median RPM and chromosome copy numbers were estimated for each sample based on the chromosome median of this bin-wise RPM ratio ($\log_2$). A cut-off of 0.6 or -0.6 was chosen to determine a higher or lower chromosome copy number than the other chromosomes in the same sample.

Pulsed-field gel electrophoresis

Exponentially growing cultures corresponding to 25 OD_{600nm} units were collected by centrifugation at 5,000 rpm for 5 min and subsequently washed in 20 mL of 10 mM Tris-HCl, 50 mM EDTA, pH 7.5. Cells were resuspended in 500 µL spheroblasting buffer (0.056 M sodium phosphate, 0.2 M EDTA, 40 mM DTT) and preheated to 42 °C on a heat block. 2 % (w/v) low-melting point agarose in H_2O was boiled and kept at 42 °C, and 500 µL (1:1) were mixed with the cells in spheroblasting buffer. 90-100 µL of the mix were pipetted into each plug mold (gives 10-12 plugs per sample). Once solidified at 4 °C, the plugs of each strain were

transferred to large Falcons (50 mL) containing 3 mL of spheroblasting buffer supplemented with 0.08 mg/mL zymolyase. Plugs were incubated for 24 h at 37 °C, shaking. The plugs were washed with 10 mL 1 x TE buffer. Subsequently, 2 mL of Proteinase K buffer (10 mM Tris-HCl, 0.42 M EDTA, 1 % N-lauroyl sarcosine, 2 mg/mL Proteinase K) were added and the plugs were incubated for a further 24 h at 50 °C, shaking. The plugs were washed five times with 10 mL of 10 mM Tris-HCl, 50 mM EDTA, pH 7.5. Plugs were stored in the same buffer at 4 °C until analysis. For the analysis, plugs were loaded on a 1 % agarose gel and sealed with 1 % agarose. Molecular weight marker CHEF DNA Size Marker #1703605 (Bio-Rad) was used. The gel was run in a CHEF-DR® III system using the following settings: initial switch time 60 sec, final switch time 120 sec, run time 24 h, 6 volts/cm, included angle 120°. The gel was stained with ethidium bromide (1.25 µg/mL in TBE) for 30 min and destained for 10 min before imaging on a ChemiDoc™ Touch imaging system (Bio-Rad).

Hsp104-GFP microscopy

Overnight cultures were grown in YPD media at 25 °C. Cultures were diluted to 0.2 OD_{600nm} units in 5 mL YPD media, and were grown for 3 h at 25 °C and afterwards shifted to 37 °C. One mL of liquid culture was collected per time point by centrifugation at 3,000 rpm for 3 min. Cells were fixed for 10 min at room temperature in Fixation solution (0.027 M K_2HPO_4, 0.073 M KH_2PO_4, 2.5 % formaldehyde, pH 6.4), washed twice with Potassium phosphate buffer 1 (0.038 M K_2HPO_4, 0.062 M KH_2PO_4, pH 6.6), and stored in Potassium phosphate buffer 2 (0.08 M K_2HPO_4, 0.02 M KH_2PO_4, pH 7.4) at 4 °C. Prior to microscopy, cells were permeabilized with 80 % ethanol for 10 min at room temperature, and resuspended in 500 µL Potassium phosphate buffer 2 containing 0.5 µg/mL DAPI (Sigma-Aldrich). Samples were loaded onto Concavanin A (Sigma-Aldrich) pre-coated 96-well plates (CellCarrier®, PerkinElmer).

Imaging was performed using High-Content Screening Opera Phenix™ microscope (PerkinElmer) in confocal mode, using a water objective with 63x magnification. Fifteen independent fields with five planes each were imaged for each sample. Acquired images were analysed with Harmony High-Content Imaging and Analysis Software (version 4.4, PerkinElmer) using standard building blocks. First, nuclei were identified with algorithm M based on the DAPI signal. Second, cytoplasm was identified with algorithm A based on GFP signal. Cellular morphology properties were calculated with standard built-in algorithm, and cell roundness was set to 65 %. Spot detection of GFP foci was performed in the cytoplasm region of the cell with algorithm C. Cells on the periphery of images were excluded from

analysis. We analysed data on the single cell level, with at least 3,000 cells per sample. The percentage of cell population that had Hsp104-GFP foci was calculated using Microsoft Excel 2013, and the data were visualized with the Prism 7.02 software package (GraphPad). Representative images were processed using ImageJ 1.52g software.

Growth curve assay and statistical analysis

Overnight cultures were grown in YPD media at 30 °C, afterwards the OD_{600nm} was measured in 100 µL culture volume in 96 well plate (Tissue culture plate, Falcon®) using Spark® microplate reader (TECAN). The cultures were diluted in 3 technical replicates to 0.05 OD_{600nm} units in 100 µL YPD with addition of either DMSO, or respective drugs. Cultures were grown at 30 °C overnight with orbital shaking in a 96 well plate (Tissue culture plate, Falcon®) in the Spark® microplate reader, and the growth dynamics of the cultures was monitored by measuring OD_{600nm} every hour. The population doubling time was calculated from an average values of technical replicates at the exponential part of the growth curve using an algorithm from (Roth V. 2006), Doubling Time Computing, available from: http://www.doubling-time.com/compute.php

For the statistical analysis, groups were randomly downsampled to the size of the smallest group. The normality of the data was tested using the Shapiro-Wilk test, and to test for homogeneity of variances, the Fligner-Killeen test was applied. Because the data were neither normally distributed nor had equal variances, the Scheirer-Ray-Hare test (an extension of the Kruskal-Wallis test and, thus, a non-parametric alternative to the two-way ANOVA [76]) was applied and followed by Dunn's post-hoc test. For all pairwise comparisons between the groups, the Mann-Whitney U test with Bonferroni correction was applied.

Figure Legends

Figure 1 | Survival of repair-defective cells after genotoxic stress is facilitated by checkpoint adaptation. (**a**) Representative images of a plating assay. Homozygous diploids were plated onto control agar plates (YPD) or plates containing 2 μM camptothecin (CPT) and incubated at 30 °C for the indicated times. Plates contained 8 μg/mL Phloxine B to visualize cellular metabolic activity. d, days. (**b**) Quantification of colony numbers after plating as described in (a). All visible colonies formed were counted and numbers of colonies formed on CPT-containing plates were normalized to the numbers obtained from YPD plates. Data are represented as mean values and SEM of 3 independent experiments. Statistical analysis was performed using one-way ANOVA with Tukey's post-hoc test (**** is $p \leq 0.0001$). (**c**) Survival of the indicated yeast strains in response to 45 Gy of X-rays was quantified as described in (b). Of note, the cell number plated on X-ray treated plates was ten-times higher than the cell number plated on control plates or to assess cell survival in response to CPT. (**d**) and (**e**) Quantification of cell survival after CPT exposure (d) or in response to X-ray irradiation (e) as described in (b) (* is $p \leq 0.05$, ** is $p \leq 0.01$). (**f**) Yeast strains of the indicated genotypes derived from either control plates (YPD) or CPT-containing agar plates (CPT) were patched and following over-night growth in liquid YPD, spotted in serial dilutions on agar plates (YPD as a control). Plates contained the indicated genotoxic agents (2 μM CPT or 2.2 units/ L bleomycin (bleo)) or received 65 J/m^2 UV. Colony formation was monitored after 3 days at 30°C. a-c indicate biological replicates.

Figure 2 | Rapamycin prevents checkpoint adaptation. (**a**) Schematic of the adaptation assay. Following genotoxic challenge (X-ray or CPT), *rad52* mutant cells were scored for their ability to form microcolonies, i.e. undergo checkpoint adaptation (see methods for a detailed explanation). (**b**) As outlined in (a), cells of the indicated genotypes were scored for their ability to adapt in the presence of 10 nM rapamycin or DMSO after irradiation with 45 Gy. Data are represented as mean values and SEM of 5 independent experiments. Statistical analysis was performed using Kruskal-Wallis test followed by Dunn's post-hoc test (** is $p \leq 0.01$). (**c**) As described in (b), microcolony formation was assessed in response to 2 μM CPT in the presence of 10 nM rapamycin or DMSO. Data are represented as mean values with the SEM of 5 independent experiments. (**d, e**) Quantification of cell survival in the presence of the indicated drugs was performed as described in Fig. 1b. Data are represented as mean values with the SEM

of 3 independent experiments. Statistical analysis was performed using two-way ANOVA with Tukey's post-hoc test (*** is $p \leq 0.001$ and **** is $p \leq 0.0001$).

Figure 3 | Extensive loss of genetic material renders adapted cells aneuploid. (**a**) DNA content of the indicated yeast strains was assessed by flow cytometry. After colonies were formed on the indicated agar plates (YPD as control, 2 µM CPT or 45 Gy X-ray as genotoxic stress), single colonies were grown in liquid media and analysed. (**b**) Representative segmentation plots depicting chromosome copy number variation in *rad52* mutants derived from either control plates (YPD) or after genotoxic treatment (2 µM CPT or 45 Gy, respectively). The segmentation plot depicts the $\log_2$ ratio of binned reads (reads per million (RPM), y-axis) for the respective chromosome position (x-axis) normalized to the sample median number of reads per bin (RPM). Dashed horizontal lines indicate a threshold of 0.6 or -0.6, respectively, to allow the identification of chromosome loss events which are indicated in red. For more details about normalization, see methods section. (**c**) Representative microscopic images of indicated strains upon heat challenge. All strains expressed endogenous Hsp104 fused with GFP. Arrows indicate Hsp104-GFP foci, for more details on automated foci analysis see methods section. Scale bar, 10 µM. (**d**) Control strains and resistant *rad52* colonies from (c) were grown in YPD at 25 °C and exposed to 37 °C. Formation of Hsp104-GFP foci was monitored using fluorescent microscopy. At least 3000 cells per sample were imaged. Error bars indicate median with interquartile range. (**e**) Strains of the indicated genotypes from (d) were spotted in 1:10 serial dilutions on YPD plates. The right panel indicates the percentage of Hsp104-GFP foci upon shift to 37 °C, summarized in (d).

Figure 4 | Characterization of aneuploid *rad52* mutants. (**a**) Population doubling times of control and X-ray resistant *rad52* cells (all in *pdr5* background to allow MG132 uptake) was determined in a growth curve assay in YPD media containing DMSO or the indicated concentrations of MG132 at 30 °C. Data are represented as a scatter plot with indicated mean and SD. Statistical analysis was performed using the Scheirer-Ray-Hare test followed by pairwise Bonferroni-corrected Mann-Whitney-U-tests (* is $p \leq 0.05$ and ** is $p \leq 0.001$). (**b**) Population doubling times of the indicated strains in YPD media containing DMSO or the indicated concentrations of rapamycin was determined in analogy to (**a**). Data are represented as a scatter plot indicating mean values and SD and statistical analysis was performed as described in (a). (**c**) Population doubling times of control strains shown in (b) during growth in

YPD media containing only the vehicle control DMSO. Data are represented as a scatter plot with bars indicating mean and SD. For statistical analysis, Fligner-Killeen-test for heterogeneity of variances was applied (**** $p \leq 0.00001$). (**d**) Indicated strains and X-ray resistant *rad52* colonies were grown to exponential cultures in YPD at 30°C and collected at OD_{600nm} 0.6. Control cultures were either mock-treated, or treated for 15 min with 50 nM rapamycin or 25 µg/mL cyclohexamide. Whole protein lysates were separated by SDS-PAGE and membranes were probed with the indicated antibodies. (**e**) Strains expressing plasmid-encoded GFP-Atg8 were grown to exponential cultures in selective media at 30°C and monitored for autophagy induction. Treatment with 50 nM rapamycin for 1 h served as a positive control. Whole protein lysates were separated by SDS-PAGE and membranes were probed with an anti-GFP antibody.

Figure 5 | MRX promotes the growth of adapted cells. (**a**) Strains derived from either control plates (YPD) or from CPT treatment (CPT) were grown to exponential phase and treated with 2 µM CPT as indicated. Whole protein lysates were separated by SDS-PAGE and membranes were probed with the indicated antibodies to monitor DNA damage checkpoint activation. Asterisk (*) marks an unspecific band. (**b**) Quantification of cell survival in the presence of 2 µM CPT after normalization to control YPD plates. Data are represented as mean values and SEM of 3 independent experiments. Statistical analysis was performed using one-way ANOVA with Tukey's post-hoc test (* is $p \leq 0.05$ and ** is $p \leq 0.01$). (**c**) Representative images of a plating assay. Indicated strains were plated onto YPD or plates containing 2 µM CPT (all containing 8 µg/mL Phloxine B) and incubated at 30°C for the indicated times. Of note, the cell number plated on X-ray treated plates was ten-times higher compared to control plates. (**d**) Quantification of cell survival in the presence of 2 µM CPT after normalization to control YPD plates. The indicated strains were analysed both in a *DNL4*-proficient and *dnl4*-deficient genetic background. Data are represented as mean values and the error bars indicate the SEM of 3 independent experiments. Statistical analysis was performed using one-way ANOVA with Tukey's post-hoc test (**** is $p \leq 0.0001$). (**e**) Strains derived from either control plates (YPD) or plates containing 2 µM CPT were grown to exponential phase and then either mock-treated or treated with 1 mM IAA for 2 h. All strains stably expressed *GDP-AFB2* to facilitate auxin-mediated protein degradation. Whole protein lysates were separated by SDS-PAGE and membranes were probed with the indicated antibodies. (**f**) Strains of the indicated genotype were spotted in serial dilutions and imaged following 6 days of incubation at 30°C.

Figure 6 | Checkpoint-adapted cells can be targeted

DNA damage activates the DDC to allow time for repair. Rad52 is critical for the repair of DSBs in *S. cerevisiae.* Following successful repair, the checkpoint is turned off and cells can continue to proliferate, referred to as checkpoint recovery (left panel). When damage is not repaired, cells will nonetheless eventually attempt to divide even though the damage persists, by actively extinguishing the checkpoint. This is promoted by TORC1 and Cdc5, both which can be targeted by rapamycin. Following adaptation, cells lose chromosomes and acquire genotoxin resistance. The aneuploid state of these cells renders them sensitive to proteotoxic stress (MG132) and rapamycin. In the case of CPT, their drug resistance can be prevented by disabling the MRX complex.

Acknowledgements

This work was supported through a generous donation from the Chica-Heinz-Schaller foundation. We are grateful to the IMB media-lab Core Facility, the Genomics Core Facility and the use of its NextSeq500 (INST 247/870-1 FUGG), and the Microscopy Core Facility, for constant support and assistance of this study. We thank Robbie Loewith for Sch9 and p-Sch9 antibodies and Bernd Bukau for the Hsp104-GFP strain. BL is supported through a Heisenberg Professorship from the DFG (LU 1709/2-1). The authors declare that they do not have a conflict of interest.

References

1 Harrison, J. C. & Haber, J. E. Surviving the breakup: the DNA damage checkpoint. *Annual review of genetics* **40**, 209-235, doi:10.1146/annurev.genet.40.051206.105231 (2006).

2 Zhu, Z., Chung, W. H., Shim, E. Y., Lee, S. E. & Ira, G. Sgs1 helicase and two nucleases Dna2 and Exo1 resect DNA double-strand break ends. *Cell* **134**, 981-994, doi:10.1016/j.cell.2008.08.037 (2008).

3 Mimitou, E. P. & Symington, L. S. Sae2, Exo1 and Sgs1 collaborate in DNA double-strand break processing. *Nature* **455**, 770-774, doi:10.1038/nature07312 (2008).

4 Lee, S. E. *et al.* Saccharomyces Ku70, mre11/rad50 and RPA proteins regulate adaptation to G2/M arrest after DNA damage. *Cell* **94**, 399-409 (1998).

5 Nakada, D., Hirano, Y., Tanaka, Y. & Sugimoto, K. Role of the C terminus of Mec1 checkpoint kinase in its localization to sites of DNA damage. *Molecular biology of the cell* **16**, 5227-5235, doi:10.1091/mbc.E05-05-0405 (2005).

6 Ma, J. L., Lee, S. J., Duong, J. K. & Stern, D. F. Activation of the checkpoint kinase Rad53 by the phosphatidyl inositol kinase-like kinase Mec1. *The Journal of biological chemistry* **281**, 3954-3963, doi:10.1074/jbc.M507508200 (2006).

7 Sanchez, Y. *et al.* Regulation of RAD53 by the ATM-like kinases MEC1 and TEL1 in yeast cell cycle checkpoint pathways. *Science* **271**, 357-360 (1996).

8 Weinert, T. A., Kiser, G. L. & Hartwell, L. H. Mitotic checkpoint genes in budding yeast and the dependence of mitosis on DNA replication and repair. *Genes & development* **8**, 652-665 (1994).

9 Agarwal, R., Tang, Z., Yu, H. & Cohen-Fix, O. Two distinct pathways for inhibiting pds1 ubiquitination in response to DNA damage. *The Journal of biological chemistry* **278**, 45027-45033, doi:10.1074/jbc.M306783200 (2003).

10 Sanchez, Y. *et al.* Control of the DNA damage checkpoint by chk1 and rad53 protein kinases through distinct mechanisms. *Science* **286**, 1166-1171 (1999).

11 Hu, F. *et al.* Regulation of the Bub2/Bfa1 GAP complex by Cdc5 and cell cycle checkpoints. *Cell* **107**, 655-665 (2001).

12 Zhang, T., Nirantar, S., Lim, H. H., Sinha, I. & Surana, U. DNA damage checkpoint maintains CDH1 in an active state to inhibit anaphase progression. *Developmental cell* **17**, 541-551, doi:10.1016/j.devcel.2009.09.006 (2009).

13 Cheng, L., Hunke, L. & Hardy, C. F. Cell cycle regulation of the Saccharomyces cerevisiae polo-like kinase cdc5p. *Molecular and cellular biology* **18**, 7360-7370 (1998).

14 Lee, K. S. & Erikson, R. L. Plk is a functional homolog of Saccharomyces cerevisiae Cdc5, and elevated Plk activity induces multiple septation structures. *Molecular and cellular biology* **17**, 3408-3417 (1997).

15 Edenberg, E. R., Vashisht, A., Benanti, J. A., Wohlschlegel, J. & Toczyski, D. P. Rad53 downregulates mitotic gene transcription by inhibiting the transcriptional activator Ndd1. *Molecular and cellular biology* **34**, 725-738, doi:10.1128/MCB.01056-13 (2014).

16 Gasch, A. P. *et al.* Genomic expression responses to DNA-damaging agents and the regulatory role of the yeast ATR homolog Mec1p. *Molecular biology of the cell* **12**, 2987-3003 (2001).

17 Zhao, X., Chabes, A., Domkin, V., Thelander, L. & Rothstein, R. The ribonucleotide reductase inhibitor Sml1 is a new target of the Mec1/Rad53 kinase cascade during growth and in response to DNA damage. *The EMBO journal* **20**, 3544-3553, doi:10.1093/emboj/20.13.3544 (2001).

18 Mathiasen, D. P. & Lisby, M. Cell cycle regulation of homologous recombination in Saccharomyces cerevisiae. *FEMS microbiology reviews* **38**, 172-184, doi:10.1111/1574-6976.12066 (2014).

19 Valencia, M. *et al.* NEJ1 controls non-homologous end joining in Saccharomyces cerevisiae. *Nature* **414**, 666-669, doi:10.1038/414666a (2001).

20 Kegel, A., Sjostrand, J. O. & Astrom, S. U. Nej1p, a cell type-specific regulator of nonhomologous end joining in yeast. *Current biology : CB* **11**, 1611-1617 (2001).

21 Frank-Vaillant, M. & Marcand, S. NHEJ regulation by mating type is exercised through a novel protein, Lif2p, essential to the ligase IV pathway. *Genes & development* **15**, 3005-3012, doi:10.1101/gad.206801 (2001).

22 Sugiyama, T., Zaitseva, E. M. & Kowalczykowski, S. C. A single-stranded DNA-binding protein is needed for efficient presynaptic complex formation by the Saccharomyces cerevisiae Rad51 protein. *The Journal of biological chemistry* **272**, 7940-7945 (1997).

23 Sugiyama, T. & Kowalczykowski, S. C. Rad52 protein associates with replication protein A (RPA)-single-stranded DNA to accelerate Rad51-mediated displacement of RPA and presynaptic complex formation. *The Journal of biological chemistry* **277**, 31663-31672, doi:10.1074/jbc.M203494200 (2002).

24 Sung, P. Function of yeast Rad52 protein as a mediator between replication protein A and the Rad51 recombinase. *The Journal of biological chemistry* **272**, 28194-28197 (1997).

25 Sung, P. Yeast Rad55 and Rad57 proteins form a heterodimer that functions with replication protein A to promote DNA strand exchange by Rad51 recombinase. *Genes & development* **11**, 1111-1121 (1997).

26 Godin, S. *et al.* The Shu complex interacts with Rad51 through the Rad51 paralogues Rad55-Rad57 to mediate error-free recombination. *Nucleic acids research* **41**, 4525-4534, doi:10.1093/nar/gkt138 (2013).

27 Bernstein, K. A. *et al.* The Shu complex, which contains Rad51 paralogues, promotes DNA repair through inhibition of the Srs2 anti-recombinase. *Molecular biology of the cell* **22**, 1599-1607, doi:10.1091/mbc.E10-08-0691 (2011).

28 Mine-Hattab, J. & Rothstein, R. DNA in motion during double-strand break repair. *Trends in cell biology* **23**, 529-536, doi:10.1016/j.tcb.2013.05.006 (2013).

29 Pellicioli, A., Lee, S. E., Lucca, C., Foiani, M. & Haber, J. E. Regulation of Saccharomyces Rad53 checkpoint kinase during adaptation from DNA damage-induced G2/M arrest. *Molecular cell* **7**, 293-300 (2001).

30 Leroy, C. *et al.* PP2C phosphatases Ptc2 and Ptc3 are required for DNA checkpoint inactivation after a double-strand break. *Molecular cell* **11**, 827-835 (2003).

31 Toczyski, D. P., Galgoczy, D. J. & Hartwell, L. H. CDC5 and CKII control adaptation to the yeast DNA damage checkpoint. *Cell* **90**, 1097-1106 (1997).

32 Sandell, L. L. & Zakian, V. A. Loss of a yeast telomere: arrest, recovery, and chromosome loss. *Cell* **75**, 729-739 (1993).

33 Clemenson, C. & Marsolier-Kergoat, M. C. DNA damage checkpoint inactivation: adaptation and recovery. *DNA repair* **8**, 1101-1109, doi:10.1016/j.dnarep.2009.04.008 (2009).

34 Galgoczy, D. J. & Toczyski, D. P. Checkpoint adaptation precedes spontaneous and damage-induced genomic instability in yeast. *Molecular and cellular biology* **21**, 1710-1718, doi:10.1128/MCB.21.5.1710-1718.2001 (2001).

35 Coutelier, H. *et al.* Adaptation to DNA Damage Checkpoint in Senescent Telomerase-Negative Cells Promotes Genome Instability. (In Press).

36 Yoo, H. Y., Kumagai, A., Shevchenko, A., Shevchenko, A. & Dunphy, W. G. Adaptation of a DNA replication checkpoint response depends upon inactivation of Claspin by the Polo-like kinase. *Cell* **117**, 575-588 (2004).

37 Syljuasen, R. G., Jensen, S., Bartek, J. & Lukas, J. Adaptation to the ionizing radiation-induced G2 checkpoint occurs in human cells and depends on checkpoint kinase 1 and Polo-like kinase 1 kinases. *Cancer research* **66**, 10253-10257, doi:10.1158/0008-5472.CAN-06-2144 (2006).

38 Carballo, J. A., Pincheira, J. & de la Torre, C. The G2 checkpoint activated by DNA damage does not prevent genome instability in plant cells. *Biological research* **39**, 331-340, doi:/S0716-97602006000200015 (2006).

39 Swift, L. H. & Golsteyn, R. M. Cytotoxic amounts of cisplatin induce either checkpoint adaptation or apoptosis in a concentration-dependent manner in cancer cells. *Biology of the cell / under the auspices of the European Cell Biology Organization* **108**, 127-148, doi:10.1111/boc.201500056 (2016).

40 Kubara, P. M. *et al.* Human cells enter mitosis with damaged DNA after treatment with pharmacological concentrations of genotoxic agents. *The Biochemical journal* **446**, 373-381, doi:10.1042/BJ20120385 (2012).

41 Liang, H. *et al.* Homeostatic control of polo-like kinase-1 engenders non-genetic heterogeneity in G2 checkpoint fidelity and timing. *Nature communications* **5**, 4048, doi:10.1038/ncomms5048 (2014).

42 Syljuasen, R. G. Checkpoint adaptation in human cells. *Oncogene* **26**, 5833-5839, doi:10.1038/sj.onc.1210402 (2007).

43 Klermund, J., Bender, K. & Luke, B. High nutrient levels and TORC1 activity reduce cell viability following prolonged telomere dysfunction and cell cycle arrest. *Cell reports* **9**, 324-335, doi:10.1016/j.celrep.2014.08.053 (2014).

44 Tatchell, K., Makrantoni, V., Stark, M. J. & Robinson, L. C. Temperature-sensitive ipl1-2/Aurora B mutation is suppressed by mutations in TOR complex 1 via the Glc7/PP1 phosphatase. *Proceedings of the National Academy of Sciences of the United States of America* **108**, 3994-3999, doi:10.1073/pnas.1014406108 (2011).

45 Mortimer, R. K., Contopoulou, R. & Schild, D. Mitotic chromosome loss in a radiation-sensitive strain of the yeast Saccharomyces cerevisiae. *Proceedings of the National Academy of Sciences of the United States of America* **78**, 5778-5782 (1981).

46 Torres, E. M. *et al.* Identification of aneuploidy-tolerating mutations. *Cell* **143**, 71-83, doi:10.1016/j.cell.2010.08.038 (2010).

47 Torres, E. M. *et al.* Effects of aneuploidy on cellular physiology and cell division in haploid yeast. *Science* **317**, 916-924, doi:10.1126/science.1142210 (2007).

48 Tang, Y. C., Williams, B. R., Siegel, J. J. & Amon, A. Identification of aneuploidy-selective antiproliferation compounds. *Cell* **144**, 499-512, doi:10.1016/j.cell.2011.01.017 (2011).

49 Oromendia, A. B., Dodgson, S. E. & Amon, A. Aneuploidy causes proteotoxic stress in yeast. *Genes & development* **26**, 2696-2708, doi:10.1101/gad.207407.112 (2012).

50 Donnelly, N., Passerini, V., Durrbaum, M., Stingele, S. & Storchova, Z. HSF1 deficiency and impaired HSP90-dependent protein folding are hallmarks of aneuploid human cells. *The EMBO journal* **33**, 2374-2387, doi:10.15252/embj.201488648 (2014).

51 Beach, R. R. *et al.* Aneuploidy Causes Non-genetic Individuality. *Cell* **169**, 229-242 e221, doi:10.1016/j.cell.2017.03.021 (2017).

52 Thorburn, R. R. *et al.* Aneuploid yeast strains exhibit defects in cell growth and passage through START. *Molecular biology of the cell* **24**, 1274-1289, doi:10.1091/mbc.E12-07-0520 (2013).

53 Stingele, S. *et al.* Global analysis of genome, transcriptome and proteome reveals the response to aneuploidy in human cells. *Molecular systems biology* **8**, 608, doi:10.1038/msb.2012.40 (2012).

54 Passerini, V. *et al.* The presence of extra chromosomes leads to genomic instability. *Nature communications* **7**, 10754, doi:10.1038/ncomms10754 (2016).

55 Blank, H. M., Sheltzer, J. M., Meehl, C. M. & Amon, A. Mitotic entry in the presence of DNA damage is a widespread property of aneuploidy in yeast. *Molecular biology of the cell* **26**, 1440-1451, doi:10.1091/mbc.E14-10-1442 (2015).

56 Hsiang, Y. H., Lihou, M. G. & Liu, L. F. Arrest of replication forks by drug-stabilized topoisomerase I-DNA cleavable complexes as a mechanism of cell killing by camptothecin. *Cancer research* **49**, 5077-5082 (1989).

57 Minois, N., Frajnt, M., Wilson, C. & Vaupel, J. W. Advances in measuring lifespan in the yeast Saccharomyces cerevisiae. *Proceedings of the National Academy of Sciences of the United States of America* **102**, 402-406, doi:10.1073/pnas.0408332102 (2005).

58 Dotiwala, F. *et al.* DNA damage checkpoint triggers autophagy to regulate the initiation of anaphase. *Proceedings of the National Academy of Sciences of the United States of America* **110**, E41-49, doi:10.1073/pnas.1218065109 (2013).

59 Keeney, S. Mechanism and control of meiotic recombination initiation. *Current topics in developmental biology* **52**, 1-53 (2001).

60 Bonney, M. E., Moriya, H. & Amon, A. Aneuploid proliferation defects in yeast are not driven by copy number changes of a few dosage-sensitive genes. *Genes & development* **29**, 898-903, doi:10.1101/gad.261743.115 (2015).

61 Sheltzer, J. M. *et al.* Aneuploidy drives genomic instability in yeast. *Science* **333**, 1026-1030, doi:10.1126/science.1206412 (2011).

62 Urban, J. *et al.* Sch9 is a major target of TORC1 in Saccharomyces cerevisiae. *Molecular cell* **26**, 663-674, doi:10.1016/j.molcel.2007.04.020 (2007).

63 Lopes, M. *et al.* The DNA replication checkpoint response stabilizes stalled replication forks. *Nature* **412**, 557-561, doi:10.1038/35087613 (2001).

64 Huang, M., Zhou, Z. & Elledge, S. J. The DNA replication and damage checkpoint pathways induce transcription by inhibition of the Crt1 repressor. *Cell* **94**, 595-605 (1998).

65 Coic, E., Feldman, T., Landman, A. S. & Haber, J. E. Mechanisms of Rad52-independent spontaneous and UV-induced mitotic recombination in Saccharomyces cerevisiae. *Genetics* **179**, 199-211, doi:10.1534/genetics.108.087189 (2008).

66 Ma, J. L., Kim, E. M., Haber, J. E. & Lee, S. E. Yeast Mre11 and Rad1 proteins define a Ku-independent mechanism to repair double-strand breaks lacking overlapping end sequences. *Molecular and cellular biology* **23**, 8820-8828 (2003).

67 Sun, C. K. *et al.* Phosphorylation of ribosomal protein S6 confers PARP inhibitor resistance in BRCA1-deficient cancers. *Oncotarget* **5**, 3375-3385, doi:10.18632/oncotarget.1952 (2014).

68 Osoegawa, A., Gills, J. J., Kawabata, S. & Dennis, P. A. Rapamycin sensitizes cancer cells to growth inhibition by the PARP inhibitor olaparib. *Oncotarget* **8**, 87044-87053, doi:10.18632/oncotarget.19667 (2017).

69 Li, J. *et al.* Targeting Plk1 to Enhance Efficacy of Olaparib in Castration-Resistant Prostate Cancer. *Molecular cancer therapeutics* **16**, 469-479, doi:10.1158/1535-7163.MCT-16-0361 (2017).

70 Williams, B. R. *et al.* Aneuploidy affects proliferation and spontaneous immortalization in mammalian cells. *Science* **322**, 703-709, doi:10.1126/science.1160058 (2008).

71 Nakashima, A. *et al.* The yeast Tor signaling pathway is involved in G2/M transition via polo-kinase. *PloS one* **3**, e2223, doi:10.1371/journal.pone.0002223 (2008).

72 Torres, E. M., Williams, B. R. & Amon, A. Aneuploidy: cells losing their balance. *Genetics* **179**, 737-746, doi:10.1534/genetics.108.090878 (2008).

73 Li, H. & Durbin, R. Fast and accurate long-read alignment with Burrows-Wheeler transform. *Bioinformatics* **26**, 589-595, doi:10.1093/bioinformatics/btp698 (2010).

74 Li, H. *et al.* The Sequence Alignment/Map format and SAMtools. *Bioinformatics* **25**, 2078-2079, doi:10.1093/bioinformatics/btp352 (2009).

75 Ha, G. *et al.* Integrative analysis of genome-wide loss of heterozygosity and monoallelic expression at nucleotide resolution reveals disrupted pathways in triple-negative breast cancer. *Genome research* **22**, 1995-2007, doi:10.1101/gr.137570.112 (2012).

76 Scheirer, C. J., Ray, W. S. & Hare, N. Analysis of Ranked Data Derived from Completely Randomized Factorial Designs. *Biometrics* **32**, 429-434, doi:Doi 10.2307/2529511 (1976).

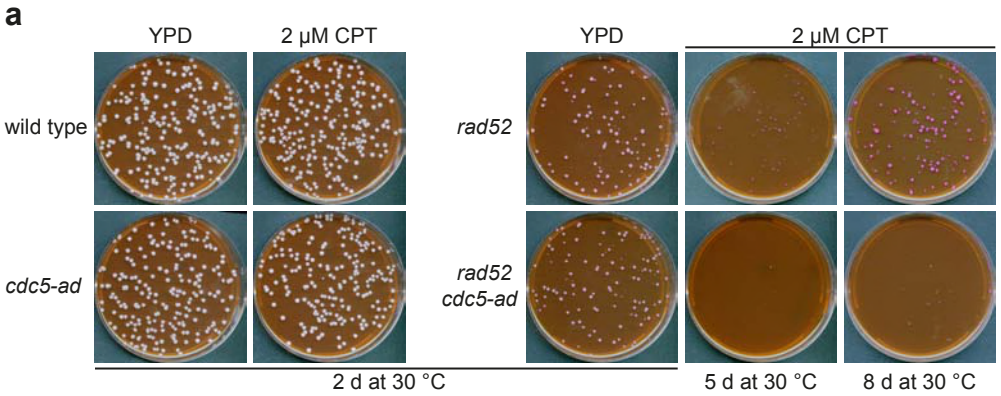
a
YPD
2 μM CPT
YPD
2 μM CPT
wild type
rad52
cdc5-ad
rad52 cdc5-ad
2 d at 30 °C
5 d at 30 °C
8 d at 30 °C

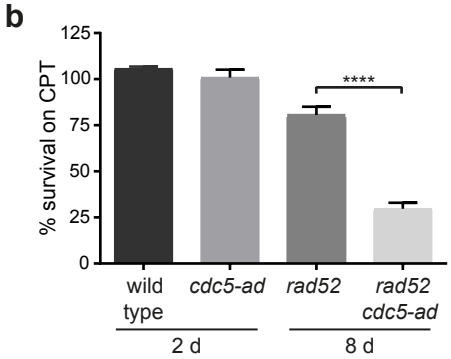
b
% survival on CPT
125
100
75
50
25
0
****
wild type
cdc5-ad
rad52
rad52 cdc5-ad
2 d
8 d

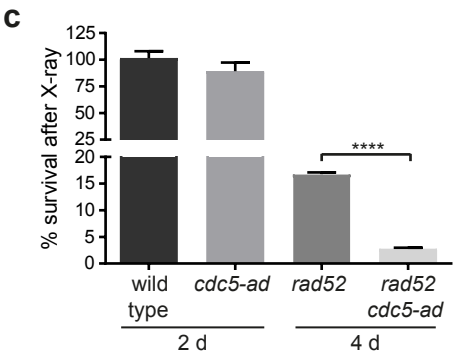
c
% survival after X-ray
125
100
75
50
25
20
15
10
5
0
****
wild type
cdc5-ad
rad52
rad52 cdc5-ad
2 d
4 d

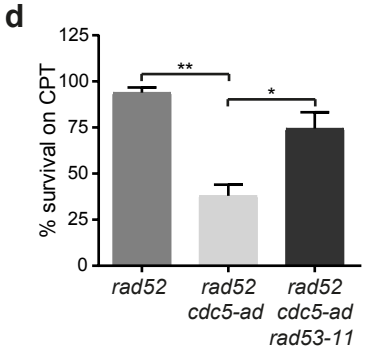
d
% survival on CPT
125
100
75
50
25
0
**
*
rad52
rad52 cdc5-ad
rad52 cdc5-ad rad53-11

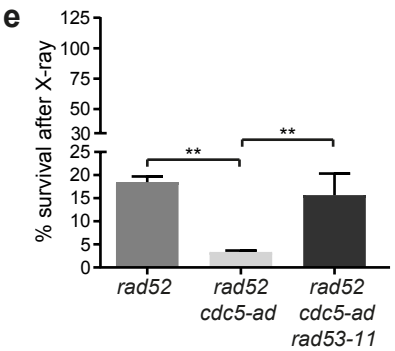
e
% survival after X-ray
125
100
75
50
30
25
20
15
10
5
0
**
**
rad52
rad52 cdc5-ad
rad52 cdc5-ad rad53-11

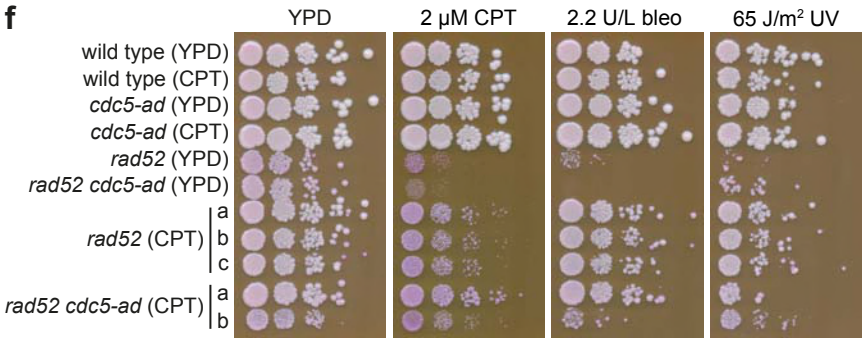
f
YPD
2 μM CPT
2.2 U/L bleo
65 J/m² UV
wild type (YPD)
wild type (CPT)
cdc5-ad (YPD)
cdc5-ad (CPT)
rad52 (YPD)
rad52 cdc5-ad (YPD)
rad52 (CPT)
a
b
c
rad52 cdc5-ad (CPT)
a
b

Figure 1.

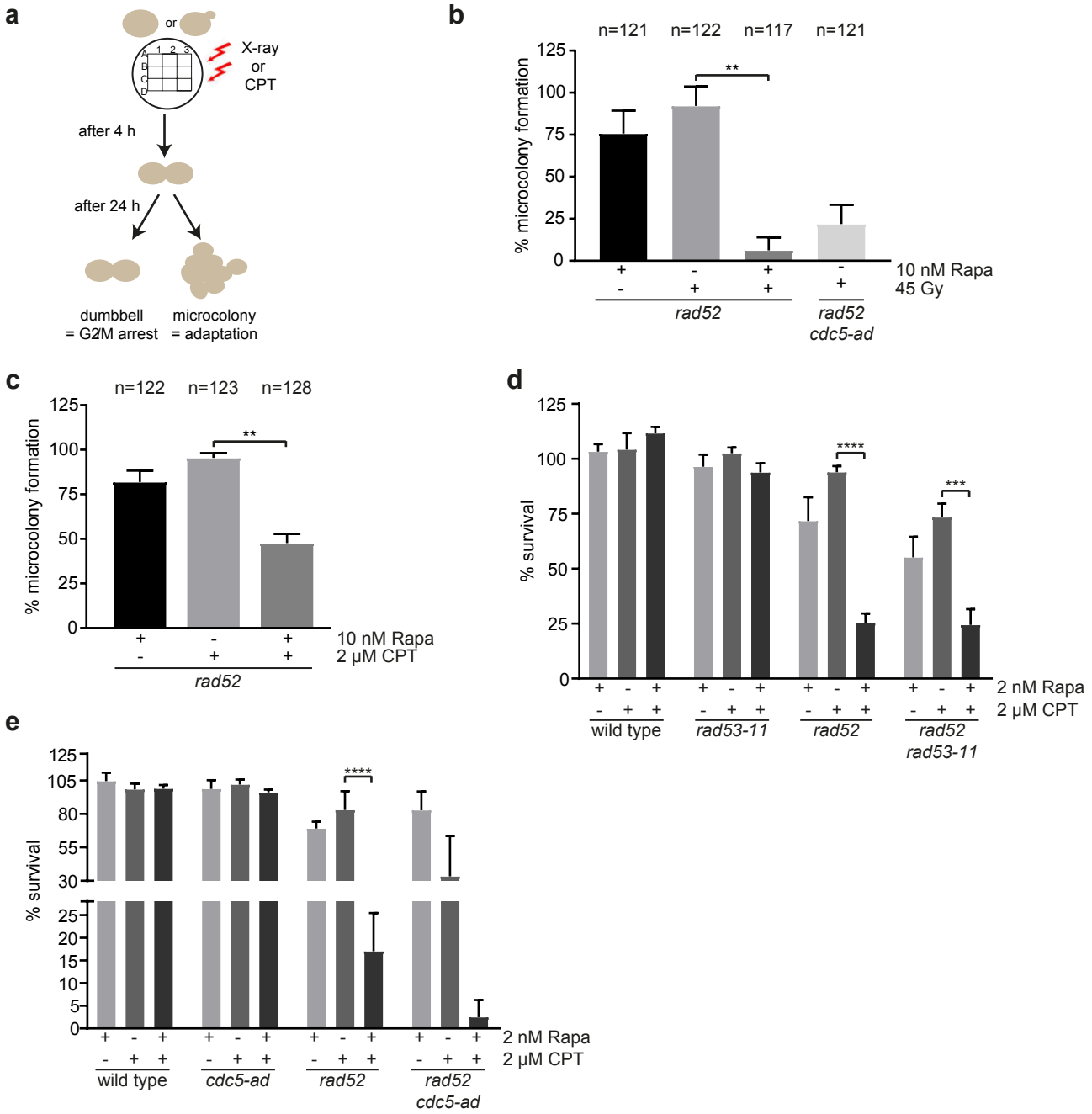
a
or
X-ray
or
CPT
after 4 h
after 24 h
dumbbell
= G2/M arrest
microcolony
= adaptation
b
n=121
n=122
n=117
n=121
% microcolony formation
10 nM Rapa
45 Gy
rad52
rad52
cdc5-ad
c
n=122
n=123
n=128
% microcolony formation
10 nM Rapa
2 μM CPT
rad52
d
% survival
2 nM Rapa
2 μM CPT
wild type
rad53-11
rad52
rad52
rad53-11
e
% survival
2 nM Rapa
2 μM CPT
wild type
cdc5-ad
rad52
rad52
cdc5-ad

Figure 2.

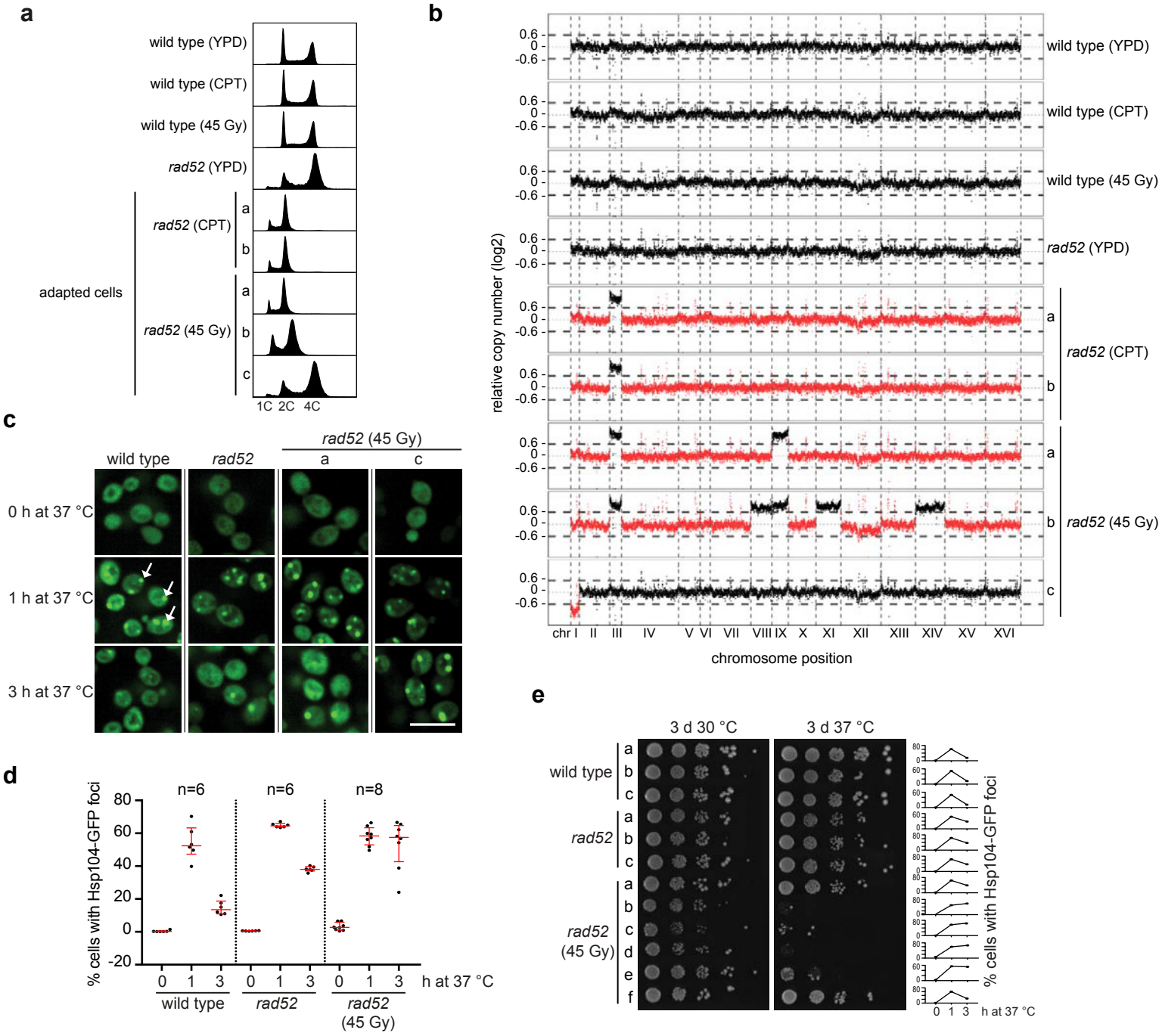
a
wild type (YPD)
wild type (CPT)
wild type (45 Gy)
rad52 (YPD)
adapted cells
rad52 (CPT)
rad52 (45 Gy)
1C 2C 4C
b
relative copy number (log2)
chromosome position
chr I II III IV V VI VII VIII IX X XI XII XIII XIV XV XVI
c
wild type
rad52
rad52 (45 Gy)
0 h at 37 °C
1 h at 37 °C
3 h at 37 °C
d
% cells with Hsp104-GFP foci
n=6
n=6
n=8
h at 37 °C
wild type
rad52
rad52 (45 Gy)
e
3 d 30 °C
3 d 37 °C
wild type
rad52
rad52 (45 Gy)
% cells with Hsp104-GFP foci
h at 37 °C

Figure 3.

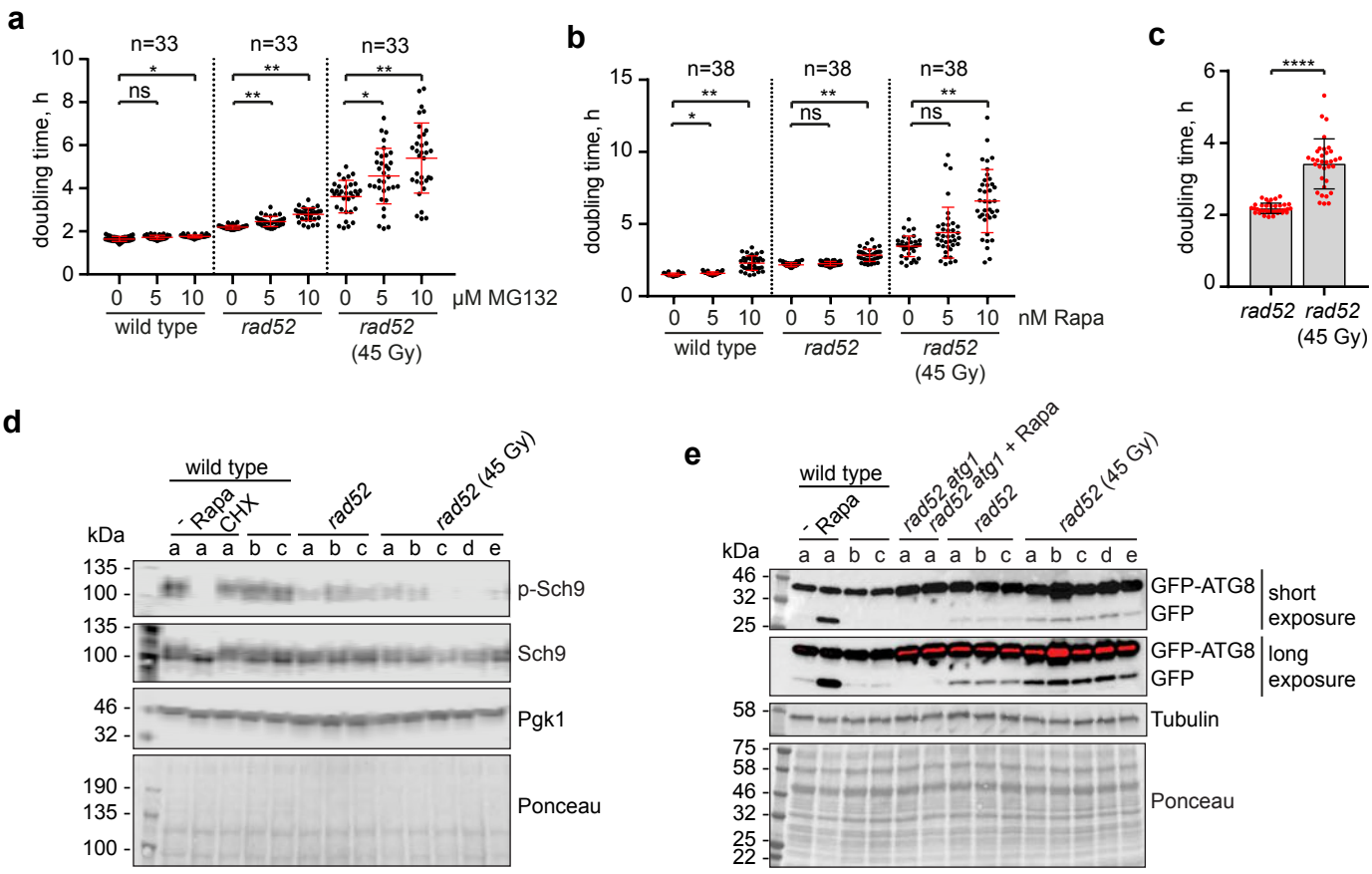
a
n=33
n=33
n=33
doubling time, h
ns
0 5 10 0 5 10 0 5 10 µM MG132
wild type
rad52
rad52 (45 Gy)
b
n=38
n=38
n=38
doubling time, h
0 5 10 0 5 10 0 5 10 nM Rapa
wild type
rad52
rad52 (45 Gy)
c
****
doubling time, h
rad52
rad52 (45 Gy)
d
wild type
- Rapa
CHX
rad52
rad52 (45 Gy)
kDa
a a a b c a b c a b c d e
p-Sch9
Sch9
Pgk1
Ponceau
e
wild type
- Rapa
rad52 atg1
rad52 atg1 + Rapa
rad52
rad52 (45 Gy)
kDa
a a b c a a a b c a b c d e
GFP-ATG8
GFP
short exposure
long exposure
Tubulin
Ponceau

Figure 4.

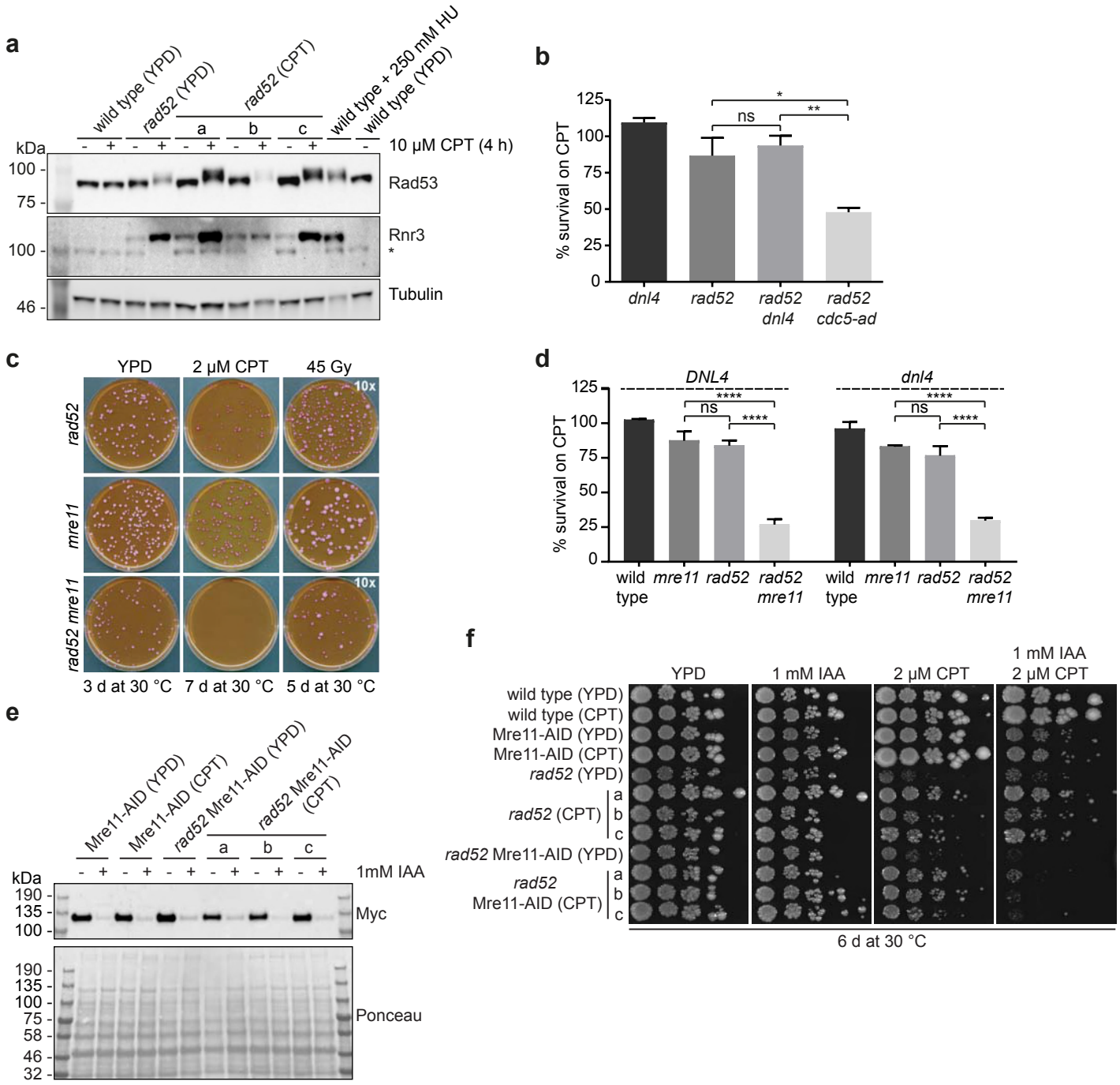
a
wild type (YPD)
rad52 (YPD)
rad52 (CPT)
a
b
c
wild type + 250 mM HU
wild type (YPD)
kDa
10 μM CPT (4 h)
100
75
Rad53
100
Rnr3
*
46
Tubulin
b
% survival on CPT
125
100
75
50
25
0
ns
*
**
dnl4
rad52
rad52 dnl4
rad52 cdc5-ad
c
YPD
2 μM CPT
45 Gy
rad52
mre11
rad52 mre11
10x
3 d at 30 °C
7 d at 30 °C
5 d at 30 °C
d
DNL4
dnl4
% survival on CPT
ns
****
wild type
mre11
rad52
rad52 mre11
e
Mre11-AID (YPD)
Mre11-AID (CPT)
rad52 Mre11-AID (YPD)
rad52 Mre11-AID (CPT)
1mM IAA
190
135
100
Myc
Ponceau
75
58
46
32
f
YPD
1 mM IAA
2 μM CPT
1 mM IAA 2 μM CPT
wild type (YPD)
wild type (CPT)
Mre11-AID (YPD)
Mre11-AID (CPT)
rad52 (YPD)
rad52 (CPT)
rad52 Mre11-AID (YPD)
rad52 Mre11-AID (CPT)
6 d at 30 °C

Figure 5.

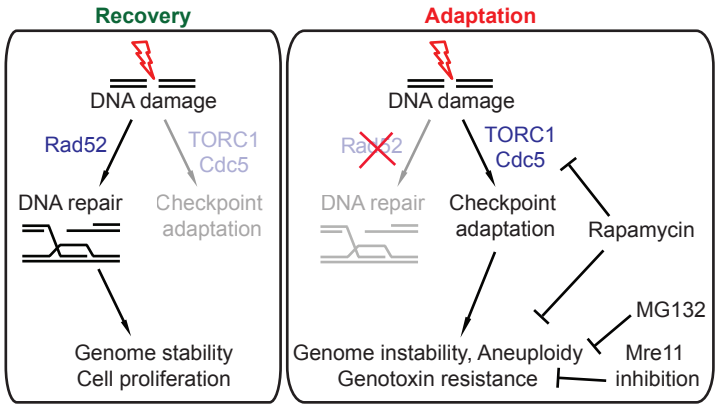
Recovery
DNA damage
Rad52
TORC1
Cdc5
DNA repair
Checkpoint
adaptation
Genome stability
Cell proliferation
Adaptation
DNA damage
Rad52
TORC1
Cdc5
DNA repair
Checkpoint
adaptation
Rapamycin
MG132
Genome instability, Aneuploidy
Genotoxin resistance
Mre11
inhibition

Figure 6.